AGU100 ADVANCING EARTH AND SPACE SCIENCE

JGR

Journal of Geophysical Research: Space Physics

RESEARCH ARTICLE

10.1029/2018JA025511

Mapping H_3^+ Temperatures in Jupiter's Northern Auroral Ionosphere Using VLT-CRIRES

R. E. Johnson[1], **H. Melin**[1], **T. S. Stallard**[1], **C. Tao**[2], **J. D. Nichols**[1], and **M. N. Chowdhury**[1]

[1]Department of Physics and Astronomy, University of Leicester, Leicester, UK, [2]National Institute of Information and Communications Technology, Tokyo, Japan

Key Points:

- High spatial resolution maps of H_3^+ temperature, column density, and total emission of Jupiter's north aurora using data from VLT-CRIRES
- The cooling and heating mechanisms in Jupiter's ionosphere are investigated by comparing the different parameters of the H_3^+ emission
- Two broad regions that change in temperature over a short period of time are observed, and their origins investigated

Correspondence to:
R. E. Johnson,
rosie.eleanor.johnson@gmail.com

Citation:
Johnson, R. E., Melin, H., Stallard, T. S., Tao, C., Nichols, J. D., & Chowdhury, M. N. (2018). Mapping H_3^+ temperatures in Jupiter's northern auroral ionosphere using VLT-CRIRES. *Journal of Geophysical Research: Space Physics*, *123*. https://doi.org/10.1029/2018JA025511

Received 23 MAR 2018
Accepted 3 JUL 2018
Accepted article online 10 JUL 2018

Abstract We present a detailed study of the H_3^+ auroral emissions at Jupiter, using data taken on 31 December 2012 with the long-slit Echelle spectrometer CRIRES (ESO-VLT). From this data set the rotational temperature of the H_3^+ ions in Jupiter's upper atmosphere was calculated using the ratio of the ν_2 Q(1,0$^-$) and ν_2 Q(3,0$^-$) fundamental emission lines. The entire northern auroral region was observed, providing a highly detailed view of ionospheric temperatures, which were mapped onto polar projections. The temperature range we derive in the northern auroral region is ~750–1000 K, which is consistent with past studies, although the temperature structure differs. We identify two broad regions which exhibit temperature changes over a short period of time (~80 minutes). We propose that the changes in temperature could be due to a local time change in particle precipitation energy, or they could be caused by dynamic temperature changes generated in the neutral thermosphere due to the magnetospheric response to a transient enhancement of solar wind dynamic pressure, as predicted by models. By comparing the H_3^+ temperature, column density, total emission, and line-of-sight velocity, we were unable to identify a single dominant mechanism responsible for the energetics in Jupiter's northern auroral region. The comparison reveals that there is complex interplay between heating by impact from particle precipitation and Joule heating, as well as cooling by the H_3^+ thermostat effect.

Plain Language Summary This study focuses on Jupiter's northern lights (aurora) and the temperature of the molecules which create them. A charged molecule, H_3^+, which exists in Jupiter's upper atmosphere, emits at infrared wavelengths. Using the Very Large Telescope, situated in Chile, we can observe Jupiter's infrared aurora. The telescope has an instrument that splits up the wavelengths of the aurora, creating spectra from which we can calculate the temperature, column density, and total emission of Jupiter's upper atmosphere. The whole polar region is observed, and maps of these parameters were created. By comparing these parameters, as well as the velocity of the charged molecules, which were calculated in our previous study, we can investigate the heating and cooling processes of Jupiter's upper atmosphere. This study is the first to measure temperature differences in Jupiter's aurora over short periods of time. These temperature changes could be caused by variations that happen during Jupiter's day or they could be caused by the response of Jupiter's magnetic field to a process external to the Jupiter system.

1. Introduction

The upper atmosphere of Jupiter can be probed by deriving the parameters of H_3^+ ions from near-infrared observations. From such observations the H_3^+ line-of-sight (LOS) velocity, temperature, column density, and total emission can be derived, providing information on Jupiter's ionosphere. The H_3^+ ions are created through a fast chain reaction that begins with ionization of molecular hydrogen, which is predominately caused by solar extreme-ultraviolet (EUV) radiation in the low-latitude regions and energetic precipitating electrons in the auroral regions. After ionization, H_2^+ quickly reacts with H_2, as molecular hydrogen is abundant in Jupiter's upper atmosphere, and produces H_3^+. Near to the homopause, H_3^+ can be destroyed by the upwelling of hydrocarbons. However, at higher altitudes the main destruction mechanism is dissociative recombination with electrons, making the lifetime of H_3^+ a function of the local electron density. At the mid-to-low latitudes, Melin and Stallard (2016) calculated that the H_3^+ lifetime was 1.6 ± 0.4 hours. This value is similar to those predicted by Achilleos et al. (1998), using the Jovian Ionospheric Model (JIM) which estimated a lifetime of ~1.05 hours. The minimum lifetime of the auroral H_3^+ is predicted to be ~10 s by JIM, although this could be longer in different regions of the aurora depending on the electron density.

H_3^+ has no allowed rotational spectrum and emits in the near-IR through ro-vibrational transitions. The ionosphere is dominated by H_3^+ at altitudes of 500–1500 km above the 1 bar level but populations of different excited vibrational states exist at different altitudes. Melin et al. (2005) modeled the peak emission of the auroral H_3^+ fundamental emission at 550 km. The overtone and hot overtone H_3^+ emission was observed at ~700–900 km and ~680–950 km respectively by Uno et al. (2014). However, these altitudes aren't fixed and vary with the precipitating electron energy, which determines the altitude at which H_3^+ ions are produced. Although the relationship between energy and H_3^+ emission is not linear, in general high energy electrons produce H_3^+ at lower altitudes than do low energy electrons (e.g.: Tao et al., 2011).

From spectroscopic observations of H_3^+ emission lines, the LOS velocity, temperature, column density, and total emission can be derived. Since H_3^+ was detected at Jupiter (Drossart et al., 1989), the temperature of the ionosphere has been measured at semi-regular intervals. At first, auroral averages were acquired, e.g.: rotational temperature of ~1250 K by Drossart et al. (1989), then studies began to expand and spatially map the global temperature (e.g. Lam et al., 1997; Miller et al., 1997). These studies also measured the column density and total emission. Recently, higher spatial and spectral resolution instruments have increased the quality of the mapping of these parameters at Jupiter (e.g.: Adriani et al., 2017; Moore et al., 2017).

Owing to the ability of H_3^+ to reradiate heat into space and thus reduce the temperature of the upper atmosphere, it has been described as a thermospheric thermostat (Miller et al., 2006). Melin et al. (2006) used a 1D self-consistent model by Grodent et al. (2001) to analyze a heating event observed by Stallard et al. (2002). They showed that the H_3^+ emission in the auroral regions can compensate for any increased particle precipitation. H_3^+ is a more efficient coolant at high temperatures; however, it may be a less efficient thermostat at high altitudes where the atmosphere significantly departs from local thermodynamic equilibrium (LTE).

By studying the H_3^+ parameters, the heating and cooling mechanisms of Jupiter's ionosphere can be investigated. Heating by impact from precipitating particles and Joule heating are candidates for the drivers of elevated temperatures measured there (Yelle & Miller, 2004). Several studies have related the drivers of heating events in Jupiter's ionosphere to a response to changes in the upstream solar wind conditions. Stallard et al. (2002) observed a heating event over 3 Earth days (~7.3 jovian days), where temperature rose by ~125 K in Jupiter's northern auroral region. They suggested that the heating was driven by an expansion of the magnetosphere caused by a decrease in the solar wind dynamic pressure. Melin et al. (2006) calculated that the heating event caused the combined ion drag energy and Joule heating rates to increase from 67 to 277 mWm^{-2}. Moore et al. (2017) observed a cooling event in Jupiter's auroral ionosphere using Keck-NIRSPEC, where the mean temperature decreased by 60 K. They used upstream IMF data acquired by the Juno-MAG instrument and propagated solar wind parameters calculated using MHD propagation models (Tao et al., 2005; Zieger et al., 2015). They found that a solar wind shock arrived at Jupiter approximately two days prior to the beginning of the cooling event, after which the solar wind was quiescent. Moore et al. (2017) suggest that the cooling event was caused by shock recovery processes, similar to those modeled by Yates et al. (2014).

Through comparison of the H_3^+ rotational temperature, column density, and total emission, the heating by impact from the auroral electron precipitation, which is the main source of ionization leading to the generation of H_3^+ at high latitudes, can be investigated. Joule heating is caused by the differing flows of neutrals and ions in Jupiter's ionosphere, which in the auroral region are caused by the magnetosphere-ionosphere coupling currents (e.g.: Cowley et al., 2005; Hill, 2001). By comparing the H_3^+ rotational temperature to the LOS velocity from Johnson et al. (2017), which was derived from the same VLT-CRIRES data set as used in this present study, we can further our understanding of the governing mechanisms in Jupiter's ionosphere.

Figure 10 in Johnson et al. (2017) illustrates the main regions of ionospheric flows identified in the study. They measured a subrotating flow of ~1.5 km s^{-1} in the planetary reference frame (PRF, a reference frame which is fixed in System III) at ~90–180° longitude in the region of the main auroral emission. This ionospheric flow is thought to be coupled to the region of magnetosphere that is subrotating due to corotation breakdown (e.g.: Cowley & Bunce, 2001; Hill, 2001; Southwood & Kivelson, 2001). A superrotational flow is identified at 180–270° longitude, with a maximum LOS velocity of ~1 km s^{-1}. Johnson et al. (2017) suggested that this flow was either due to ionosphere or magnetosphere forcing. In a reference frame which rotates with the planet, they observed very strong subrotational flows (~2.5 km s^{-1}) in a polar region with very weak infrared emission, typically described as the dark region in ultraviolet (UV) observations. These ionospheric flows deviate from neutral wind flows (assuming the neutrals are corotating) and could be an indicator of Joule heating.

In this study we derive the H_3^+ rotational temperature, column density, and total emission, and map these parameters on polar projections. We compare the H_3^+ parameters to the LOS velocity from Johnson et al. (2017), as described above. The observations of Jupiter's northern auroral region presented in this paper are outlined in Section 2. The methods used to derive the H_3^+ parameters are discussed in Section 3. The results of highly detailed polar projections of these H_3^+ parameters are presented in Section 4, and are discussed in Section 5.

2. Observations

This study uses the same data set as Johnson et al. (2017), which was taken on 31 December 2012 with VLT-CRIRES (Kaufl et al., 2004). CRIRES is a long-slit Echelle spectrometer with a very high spectral resolution ($R = \lambda/\Delta\lambda$) of ~100,000 with a slit width of 0.2″. The wavelength range of the four Aladdin spectral detector arrays of CRIRES (each 1024 spectral by 512 spatial pixels) was 3.884–3.986 μm, which means a number of H_3^+ emission lines from the Q-branch were simultaneously measured, from which the H_3^+ parameters can be derived. The slit length is 40″ and the detectors have a spatial resolution of 0.089″ per pixel.

The observer sublatitude of Jupiter at the time of the observations was +3.4°; therefore, the northern aurora was favorably displayed. Jupiter was setting during the observations, causing the air mass to increase from 1.4 to 1.6 and leading to a slight decrease in the signal-to-noise. The weather was clear and stable, with a seeing of ~0.5″, causing minimal smearing of the spectra.

During the observations, the auroral region was scanned six times with the slit of CRIRES, which was aligned West-East on Jupiter, perpendicular to the rotational axis. To scan the aurora, the slit was positioned at the polar limb, with the center of the slit at the central meridian line (CML), and then the telescope was incrementally adjusted so that the slit was stepped equatorward with a step size equivalent to the slit width (0.2″). The exposure time for the spectra taken at each position was 25 s. Six scans were taken between 02:13 and 04:15 UT on 31 December 2012, each covering a region from the polar limb of the planet through to ~45° latitude, which takes 35 steps. In addition to measuring spectra from Jupiter, calibration exposures were required for the data reduction processes, which are discussed in greater detail in Johnson et al. (2017).

3. Data Analysis

In order to determine the rotational temperature of H_3^+, this study focuses on two spectral lines, $Q(1,0^-)$ and $Q(3,0^-)$. We refer the reader to Figure 3 of Johnson et al. (2017) for an example spectrum from Jupiter's auroral and subauroral regions, which includes the H_3^+ $Q(1,0^-)$ and $Q(3,0^-)$ emission lines at ~3.95295 and ~3.98558 μm, respectively. These emission lines are in the same vibrational manifold and represent transitions from the first excited vibrational energy level to the ground state, $\nu_2 \rightarrow 0$, which is a fundamental transition (McCall, 2001).

The data were reduced in the usual way as described by Johnson et al. (2017). A Gaussian profile was fitted to every spatial position along the emission line to determine the height, width, and wavelength of the emission line at each spatial position across the observed section of Jupiter that the slit encompasses. The spectral radiance, which is the flux emitted per unit of solid angle per unit wavelength, is taken as the height of Gaussian profile. Polar projections of the $Q(1,0^-)$ and $Q(3,0^-)$ H_3^+ spectral radiances were made of Jupiter's northern aurora, using the methods outlined in Johnson et al. (2017). To increase signal-to-noise, the average spectral radiance of $Q(1,0^-)$ and $Q(3,0^-)$ was calculated from the six scans, which are shown in Figures 1a and 1b, respectively.

The rotational temperature of the H_3^+ ions in the upper atmosphere is calculated using the ratio of the spectral radiances of the $Q(1,0^-)$ and $Q(3,0^-)$ fundamental lines, given by the following equation,

$$\frac{I_{Q_1}}{I_{Q_3}} = \gamma \exp\left[\frac{(E'_{Q_3} - E'_{Q_1})}{k_B T}\right] \tag{1}$$

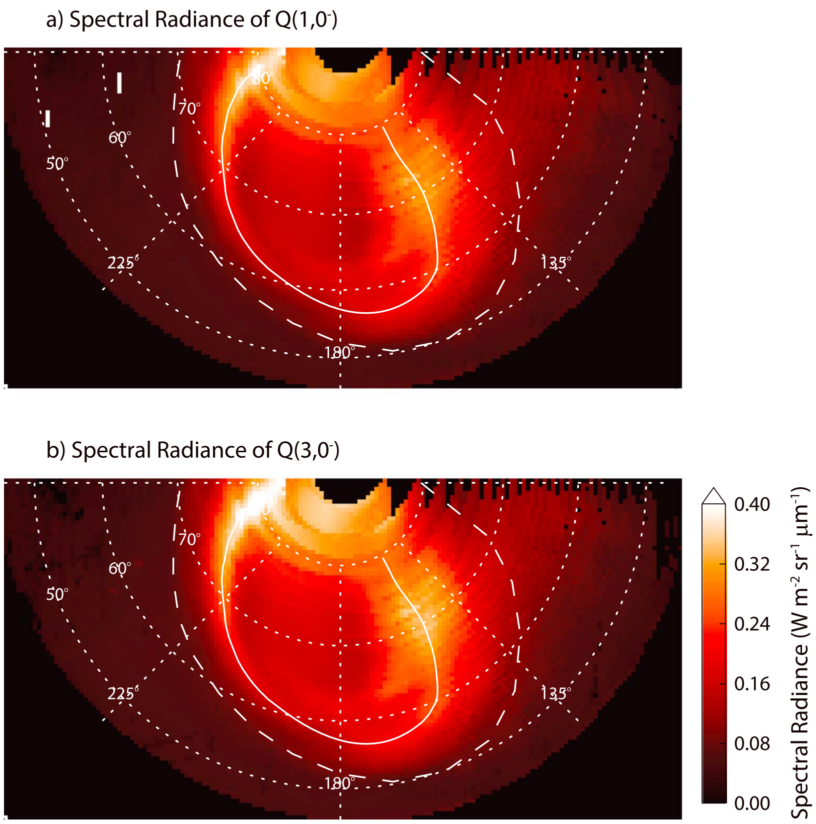

Figure 1. Polar projections of the spectral radiances of (a) Q(1,0$^-$) and (b) Q(3,0$^-$) H_3^+ emission lines. The longitudes are in System III, and the latitudes are planetocentric. The white line is the peak in H_3^+ auroral intensity along the main auroral emission, as measured by Johnson et al. (2017). The white dashed line is the magnetic footprint of Io according to the Grodent et al. (2008) model.

where

$$\gamma = \frac{g_{Q_1} \times \left(2J'_{Q_1} + 1\right) \times hc\omega_{Q_1} \times A_{Q_1}}{g_{Q_3} \times \left(2J'_{Q_3} + 1\right) \times hc\omega_{Q_3} \times A_{Q_3}} \tag{2}$$

where the subscripts Q1 and Q3 refer to Q(1,0$^-$) and Q(3,0$^-$), respectively, E' is the energy of the upper state, A the Einstein A-coefficient, g is the nuclear spin degeneracy, J' the rotational quantum number of the upper state, and ω is the transition frequency, which are taken from the theoretical spectroscopic line list of Neale et al. (1996) and shown in Table 1. The constants in this equation are the Planck constant

Table 1
Parameters Required for Deriving the Physical Parameters of H_3^+

Parameters (taken from Neale et al., 1996)	Q(1,0$^-$)	Q(3,0$^-$)
Energy of the upper state, E′	2,552.57 cm^{-1}	2,961.84 cm^{-1}
Einstein A-coefficient, A	128.7 s^{-1}	123.2 s^{-1}
Nuclear spin degeneracy, g	4	4
Rotational quantum number of the upper state, J′	3	9
Transition frequency, ω	2,529.73 cm^{-1}	2,509.08 cm^{-1}

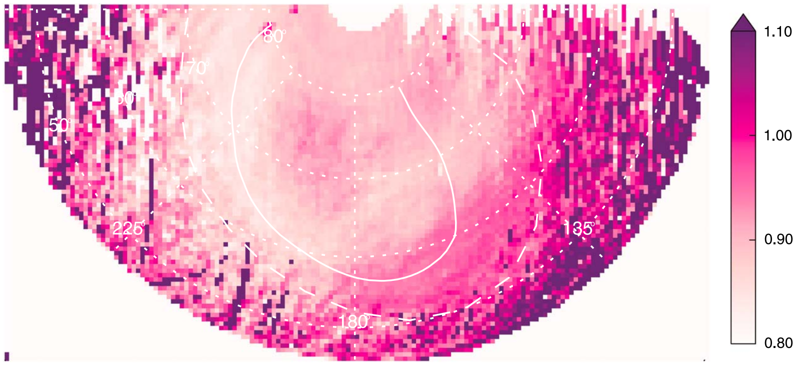

Figure 2. The ratio of the spectral radiances of the H_3^+ Q(1,0$^-$) and Q(3,0$^-$) fundamental lines. Similar format to Figure 1.

(h~6.63 × 10^{-34} m^2 kg s^{-1}), the speed of light (c~2.99 × 10^8 m s^{-1}), and the Boltzmann constant (k_B~1.38 × 10^{-23} m^2 kg s^{-2} K^{-1}).

The ratio of the average spectral radiance of Q(1,0$^-$) (Figure 1a) and Q(3,0$^-$) (Figure 1b) is shown in Figure 2. The ratio shows that Q(3,0$^-$) is generally more intense than Q(1,0$^-$) in the auroral region and changes depending on the location within the auroral region. Outside the auroral region there are some regions where the Q(1,0$^-$) emission is more intense than Q(3,0$^-$) emission; however, these coincide with regions of poor signal-to-noise, which will be discussed in greater detail in section 3.1.

Equation (1) can be rearranged to solve for temperature,

$$T = \frac{\left[E'_{Q_1} - E'_{Q_3}\right] \times 100 \times {}^{hc}\!/_{k_B}}{\ln(\gamma) - \ln\left(\frac{I(\omega_{Q_1})}{I(\omega_{Q_3})}\right)}. \tag{3}$$

Using equation (3), the ratio of Q(1,0$^-$) and Q(3,0$^-$) (Figure 2) can be converted to rotational temperature of H_3^+. The parameters are as above and given in Table 1. The factor 100 hc is needed in equation (3) to convert the energy from wave number to SI units. The temperatures are column average as the bulk of the fundamental emission occurs at ~550 km above the 1 bar level (Melin et al., 2005); however, since this altitude is based on a model we cannot resolve the exact altitude.

The column density, N(H_3^+), is the density of a column of the planet's atmosphere (of unit cross-sectional area) perpendicular to the planet's surface. It is calculated by dividing the measured intensity from the emission line (I_{obs}) by the theoretical emission per molecule from that particular line (I_{model}), described by the following equation:

$$N\left(H_3^+\right) = \frac{I_{obs}(\lambda)}{I_{model}(\lambda, T)}. \tag{4}$$

The intensity (I_{obs} [W m^{-2} sr^{-1}]), can be derived by multiplying the spectral radiance by the full width at half maximum (FWHM [μm]) of the Gaussian profile fitted to the H_3^+ emission line. The theoretical emission produced by one molecule at wavelength λ (I_{model}(λ, T) [W sr^{-1}]) can be calculated using equation (5). This requires inputs of the parameters for a particular transition, which can be taken from the line list of Neale et al. (1996), and the rotational temperatures, which were calculated above. Q(T) is the partition function of H_3^+, taken from Miller et al. (2013).

$$I_{model}(\lambda, T) = \frac{g_{if}\, J'_{if}\, \omega_{if}\, A_{if} hc \times 100}{4\pi\, Q(T)} \times \exp\left[-\frac{hc\, E'_{if} \times 100}{kT}\right] \tag{5}$$

To achieve a column density that is perpendicular to the planet's surface rather than along the LOS of the observer a correction must be performed. This correction is performed on the intensity, which experiences

 10.1029/2018JA025511

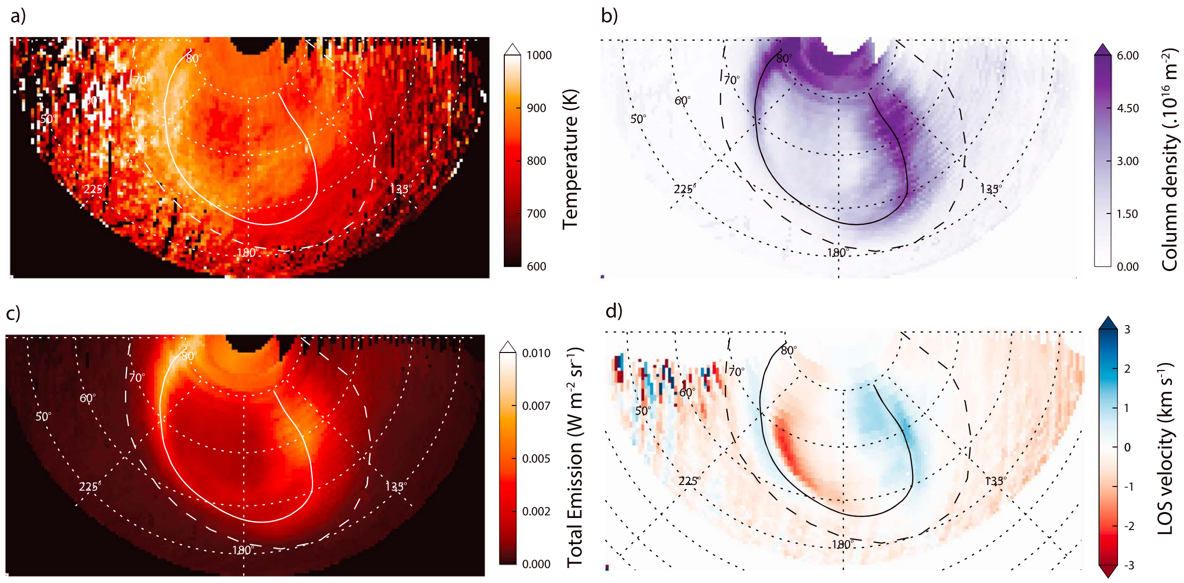

Figure 3. Polar projections of the H_3^+ (a) average rotational temperature, (b) average column density, (c) average total emission, and (d) the line-of-sight velocity in the planetary reference frame derived from IR observations of Jupiter's northern auroral region, taken on 31 December 2012. Similar format to Figure 1.

limb brightening due to an effect caused by the observer's LOS intercepting more H_3^+ emission towards the limb of Jupiter. By sequentially plotting the intensity profiles derived from the spectrum at each latitude position in the scan of the northern polar region, a 2-D intensity map was created and the limb of the planet was identified as described by Johnson et al. (2017). Following this, the distance from the center of the planet and each data point could be found and is referred to as the pathway. The LOS intensity correction value (LOS_c) is then found using a cosine function of the pathway ($r_{pathway}$) and the planetary radius ($r_{planetary\_radius}$) at the particular latitude of the pixel, as shown by equation (6). The intensity is then multiplied by this factor and subsequent column density, which is calculated from this intensity, is now effectively perpendicular to the planet's surface.

$$LOS_c = \cos\left(\frac{r_{pathway}}{r_{planetary\_radius}}\right) \tag{6}$$

The total emission, $E(H_3^+)$, is the total emission from the H_3^+ population across all possible energy transitions at a given temperature and was first introduced by Lam et al. (1997). It is calculated by multiplying the theoretical emission from all emission lines produced by one molecule ($E(\lambda,T)$) by the column density ($N(H_3^+)$), as shown by equation (7). A hemispheric emission factor of 2π steradian is needed to produce the total energy escaping the planet. The values for column density are as calculated according to the above prescription. $E(\lambda,T)$ is calculated by taking the exponential of the cooling function as defined by Miller et al. (2013).

$$E\left(H_3^+\right) = E(\lambda, T) \times N\left(H_3^+\right) \times 2\pi \tag{7}$$

Polar projections were created of the rotational temperature, column density, and total emission, shown in Figure 3.

As H_3^+ experiences ro-vibrational transitions, there is a temperature associated with rotational and vibrational as well as kinetic motions (which are also known as translational motions). If all three temperatures are equal then the H_3^+ ions are in LTE and the measured temperature is representative of the thermosphere as well as the ionosphere. Miller et al. (1990) derived a vibrational temperature of 1100 ± 100 K, which was in agreement with the rotational temperature of 1100 ± 100 K derived by Drossart et al. (1989), and therefore it seemed that H_3^+ existed under LTE conditions. However, some studies, such as Kim et al. (1992), dismissed

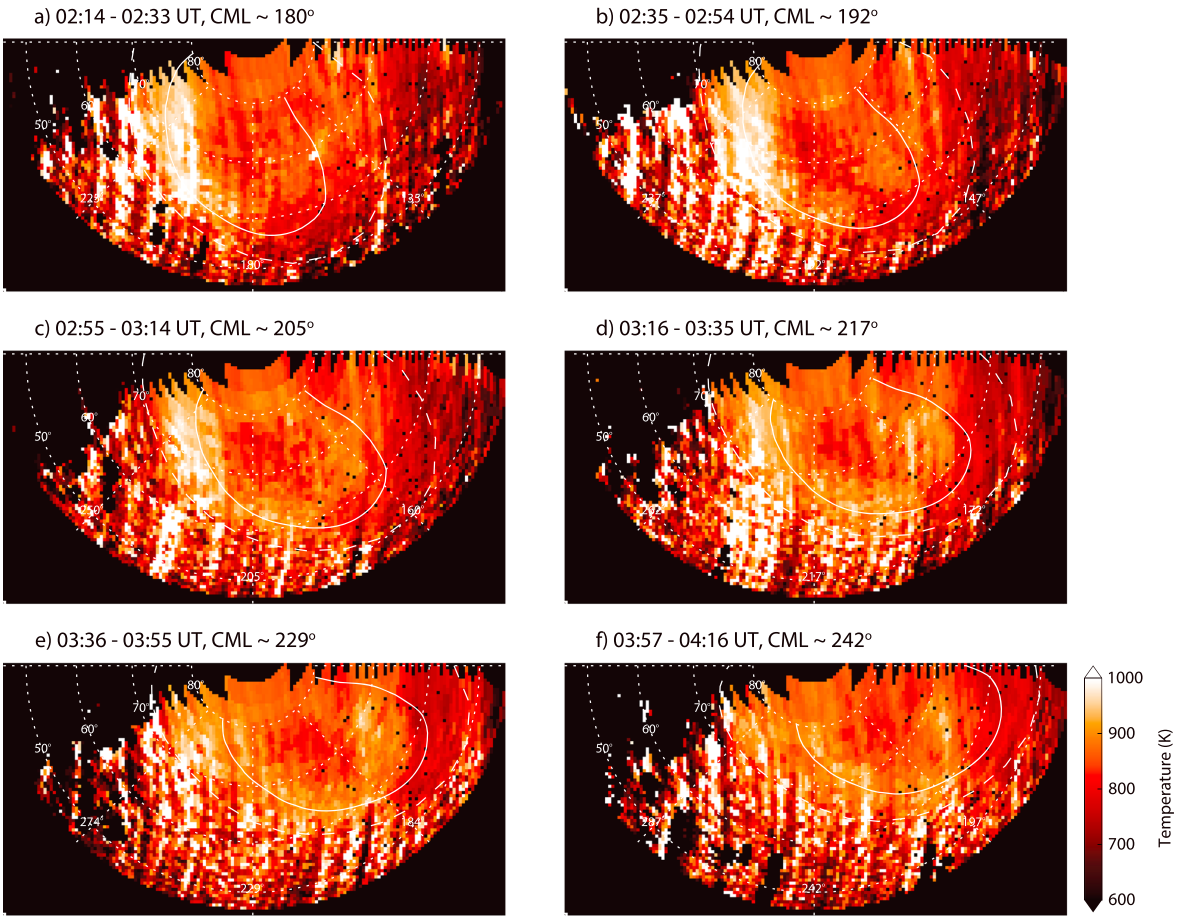

Figure 4. (a–f) Six polar projections of the H_3^+ temperature derived on 31 December 2012. Similar format to Figure 1.

this assumption. Melin et al. (2005) and Tao et al. (2011) found that non-LTE effects increase with altitude, where the temperature is higher and the density is lower. Giles et al. (2016) detected H_3^+ lines in Jupiter's auroral regions in the 5 μm window and this was the first and only study to date to measure all three temperatures simultaneously. They obtained a kinetic temperature of 1390 ± 160 K, a rotational temperature of 960 ± 40 K, and a vibrational temperature of 925 ± 25 K. These three temperature values are not all in agreement with each other, which indicates a departure from LTE. However, Melin et al. (2005) and Tao et al. (2011) show that the fundamental emission is least effected by departures from LTE. Therefore, following past studies involving the fundamental emission lines (e.g.: Miller et al., 1990), we apply the quasi-LTE assumption. By assuming quasi-LTE, we acknowledge that non-LTE effects may exist in Jupiter's upper atmosphere but they have a negligible influence on the fundamental emission. Since $Q(1,0^-)$ and $Q(3,0^-)$ are both fundamental lines, they are the least influenced by non-LTE effects, and so any temperatures derived in this study are representative of the ionosphere as well as the thermosphere.

In this study the H_3^+ temperature, column density and total emission are compared to the LOS velocity (Figure 3d) to investigate the relationship between heating, cooling, and ion velocities. For a full discussion on the LOS velocities and how they are derived, the reader is referred to Johnson et al. (2017).

In order to investigate short timescale changes in the auroral temperature, we also calculated the temperature for each of the six scans, as shown in Figure 4. The temperature calculation is very sensitive to the signal-to-noise: To make sure that any observed temperature differences were not just random fluctuations, averages were taken of the first two (Figures 4a and 4b) and last two (Figures 4e and 4f) polar projections. These averages are ~80 min and ~50° longitude apart and referred to as averages 1 and 2 for the start and

10.1029/2018JA025511

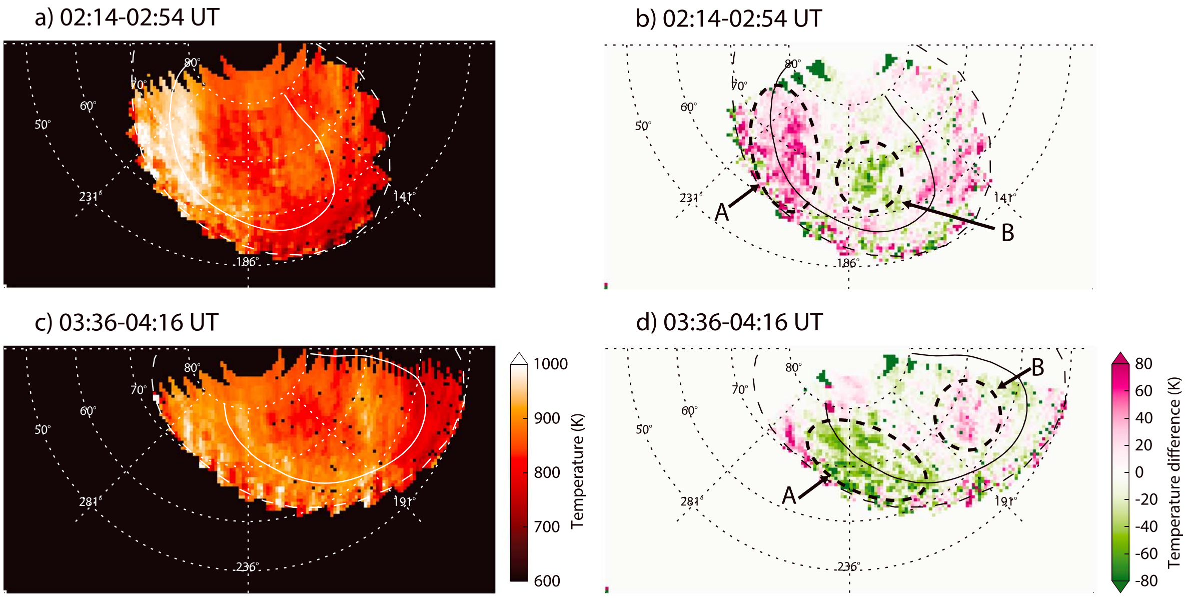

Figure 5. The average H_3^+ temperature and temperature differences at the (a and b) start and (c and d) end of the observations. The two broad regions of temperature changes, labeled A and B, are bound by dashed black lines. Similar format to Figure 1.

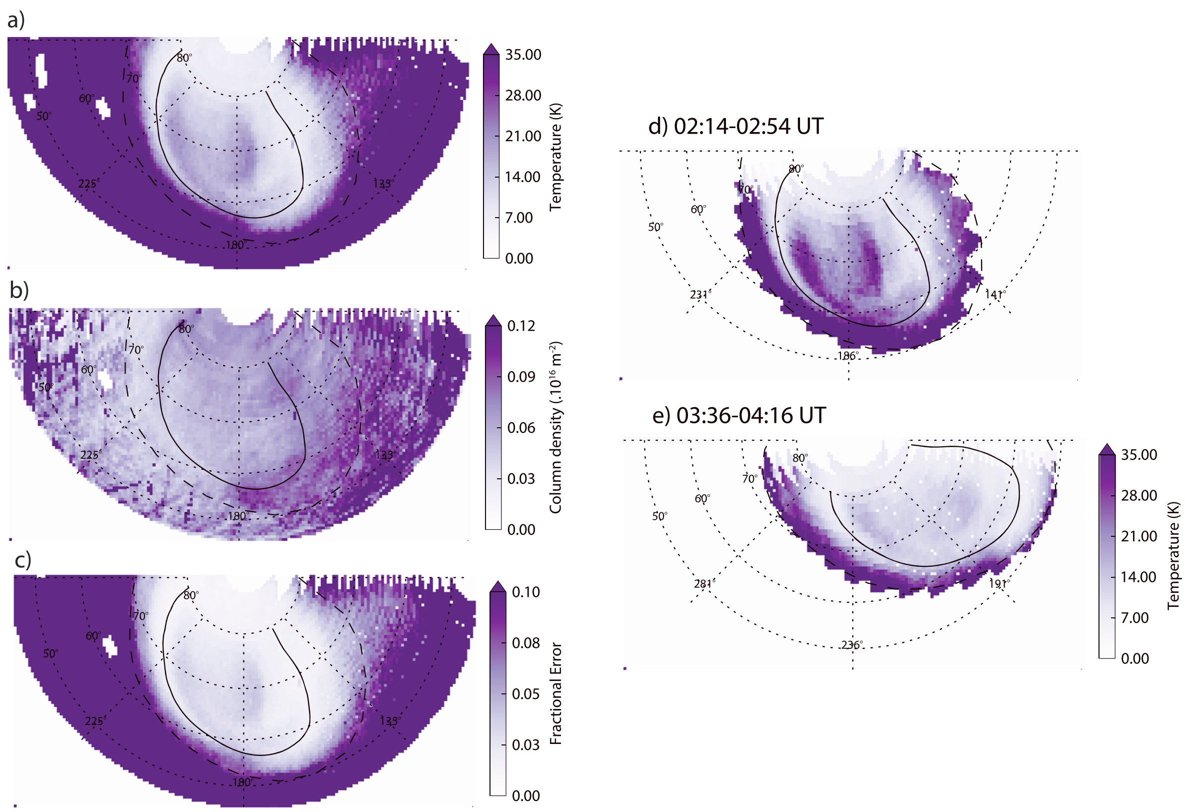

Figure 6. The error on the H_3^+ average (a) temperature, (b) column density, and (c) total emission. The temperature error for (a) average 1 and (b) average 2. Similar format to Figure 1.

end of the observations, respectively. The temperature difference was then calculated by subtracting the average over the whole of the observations (Figure 3a) from averages 1 and 2. The polar projections of averages 1 and 2, and the respective temperature differences are shown in Figure 5. Note that the above analysis was not performed on the total emission or the column density as no significant variation in these parameters was observed over the set of observations.

3.1. Errors

The errors for the parameters calculated in this study are shown in Figure 6. The errors mainly result from fitting a Gaussian to the emission lines, and these fitting errors were propagated through the calculations to produce the errors for each parameter, shown in Figures 6a–6c. Equatorward of the Io magnetic footprint, the error on all the parameters significantly increases as the signal-to-noise decreases. The difference between the $Q(1,0^-)$ and $Q(3,0^-)$ spectral radiance is very small, and therefore, the temperature calculation is very sensitive to noise altering the $Q(1,0^-)$:$Q(3,0^-)$ emission ratio. For this reason, in this study the focus will be on the values poleward of the Io footprint where signal-to-noise is above ~10.

The temperature error for averages 1 and 2 are shown in Figures 6d and 6e. The entire observed polar region is not shown in Figures 6d and 6e as the error equatorward of the Io magnetic footprint is larger than 35 K. It can be seen that the errors vary across the observations, due to an increase in noise as the air mass increased during the observations. However, in general they remain much lower than 35 K within the locus of the main auroral emission, as shown in Figures 6d and 6e.

4. Results

Figure 3 shows the key results for this paper: (a) the average H_3^+ temperature, (b) the average H_3^+ column density, and (c) the average H_3^+ total emission for the observations taken on 31 December 2012. Figure 3d shows the LOS velocity in the PRF, taken from Johnson et al. (2017). Since the LOS velocity depends on the viewing geometry, an average of the LOS velocity cannot be taken over the observations as this would lead to unphysical results. Instead, the first scan, where there is an excellent view of the northern aurora, is used in Figure 3 in order to compare to the other parameters. Figure 7 shows the parameters plotted against each other: (a) total emission versus column density, (b) temperature versus total emission, (c) temperature versus column density, and (d) temperature versus the absolute magnitude of the LOS velocity in the PRF. Only data points poleward of the Io magnetic footprint were used to produce Figure 7.

Figure 3c shows the average total emission that reaches a maximum of ~10 mW m^{-2} sr^{-1} in the region of the main auroral emission. The range of values that the total emission encompasses is in agreement with past studies. The total emission represents the total energy output from the H_3^+ emission (Lam et al., 1997), and as can be seen from Figure 3c, the majority of the energy output is in the region of the main auroral emission and the more active regions of the polar aurora. The column density is shown in Figure 3b, with values reaching a maximum of ~6×10^{16} m^{-2} in the region of the main auroral emission, driven primarily by impact ionization due to precipitating particles. By comparing Figures 3c and 3b it is possible to see that the total emission is high where the column density is large. This comparison can be seen more qualitatively in Figure 7a, where a positive correlation between total emission and column density is shown. The Pearson's correlation coefficient for the total emission and column density is ~0.98, implying a strong positive correlation.

The average temperature is shown in Figure 3a, with values in the range ~700–1,000 K, which are in agreement with past studies. Using Juno-JIRAM observations, Adriani et al. (2017) observed elevated temperatures along the main auroral oval. However, in this study the temperature structures appear to be ordered only along the main auroral emission at ~180°–270° longitude, and there is no broad region of heating at ~90°–180° like that observed by Adriani et al. (2017). Moore et al. (2017) observed higher temperatures at ~180°–270° than ~90°–180° longitude along the main auroral emission, which is in agreement with the observations in this present study, however, their spatial resolution was relatively modest.

The thermostat effect of H_3^+ can cool the auroral regions. If H_3^+ was efficiently reradiating the auroral energy into space then where the total emission is large the temperature should be low. Figure 3c (the average total emission) shows a map of where the regions of cooling should be taking place in the auroral region. By comparing Figures 3a and 3d, it can be seen that on the main auroral emission at ~180°–270° longitude, the

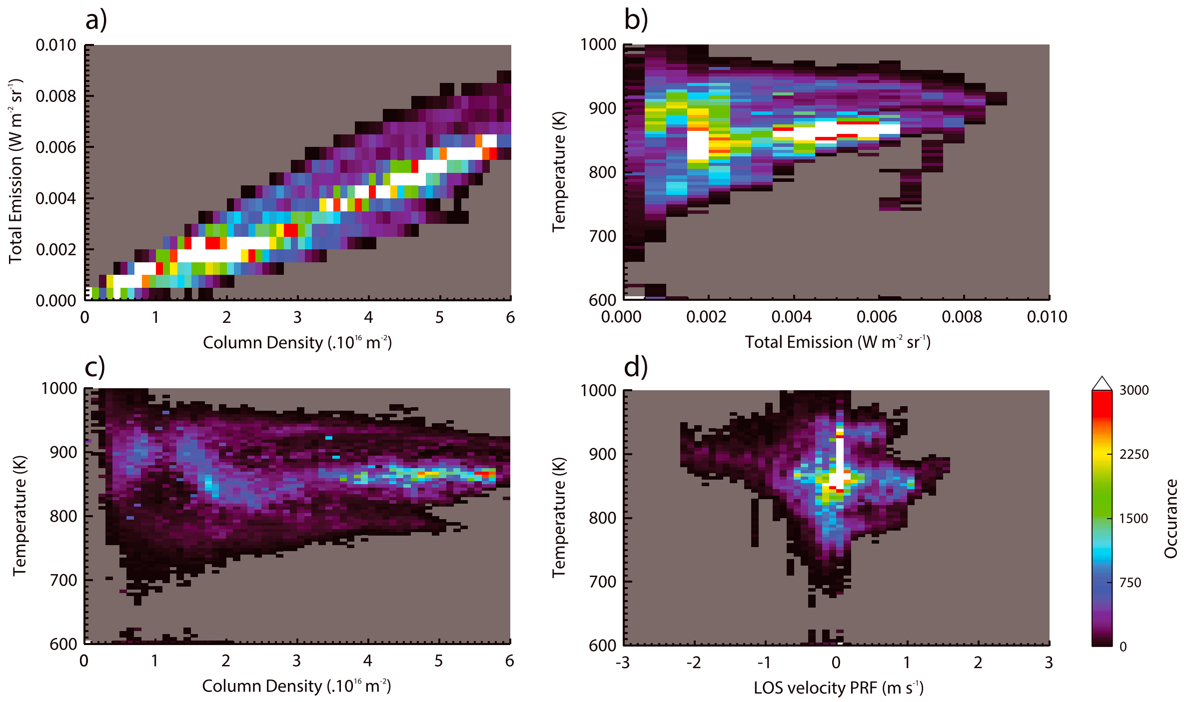

Figure 7. The correlation between parameters derived from the H_3^+ emission: (a) total emission versus column density, (b) temperature versus total emission, (c) temperature versus column density, and (d) temperature versus the absolute magnitude of the LOS velocity in the PRF. Only data points poleward of the Io magnetic footprint were included in these plots, where the Io magnetic footprint coordinates were taken from the Grodent et al. (2008) model. The gray region indicates the absence of data and the colors show the number of data points present in each bin.

aurora is bright and also hot, indicating that the rate of heating is larger than the cooling. However, there are some regions where the aurora is bright and the temperature is low, for example within ~140°–180° longitude, indicating that H_3^+ is effectively reradiating the auroral energy. Figure 7b shows the correlation of the temperature and total emission for this study. There is a high occurrence of temperatures 800–900 K within a total emission range of ~2–6 mW m^{-2} sr^{-1}. At low values of total emission in the range of ~0.5–3 mW m^{-2} sr^{-1} and temperatures in the range of ~800–950 K, there may potentially be an anticorrelation. However, overall, the Pearson's correlation coefficient is ~0.71, which implies a modest positive correlation between the temperature and total emission.

In regions where H_3^+ is denser, there is a higher rate of ionization (assuming a similar background thermosphere composition); therefore, the H_3^+ column density (Figure 3b) should show where the ionization (i.e., particle precipitation) is occurring. If heating by impact from particle precipitation is significant, it would cause elevated temperatures in regions where the column density is large. Through comparison of Figures 3b and 3a, it can be seen that there is some correlation between large column densities and large temperatures along the main auroral emission at 180°–270° longitude. However, moving from 270° towards 180° longitude along the main auroral emission, the column density decreases but the temperature remains relatively high. At 90°–180° longitude, the structure in the temperatures is very different and some regions present high temperatures but high column densities. Figure 7c shows temperature versus column density. There is a high occurrence of temperatures at ~850 K and column densities at ~4–6 × 10^{16} m^{-2}. There is a potential anticorrelation between the column densities at ~1–3 × 10^{16} m^{-2} for temperatures of ~750–900 K. However, overall, there is a modest positive correlation between temperature and column density, with a Pearson's correlation coefficient of ~0.78.

This study has an advantage over past studies because the temperature, column density, and total emission can be directly compared to the LOS velocities derived from the same data set by Johnson et al. (2017). Figure 3d shows the LOS velocities in the PRF. This reference frame is fixed in System III, and any deviation from zero implies the H_3^+ ions have a velocity greater than or less than the rotation rate of the planet. In Figure 3d, at longitudes greater than the CML value (~180°) the planet is rotating towards the observer. Therefore, positive LOS velocities (represented by blue regions) imply flows are rotating towards the observer faster than the rotation rate of the planet, that is, superrotation, and negative LOS velocities (represented by red regions) imply flows are rotating towards the observer slower than the rotation rate of the planet, that is, subrotation. At longitudes less than the CML value, where the planet is rotating away from the observer, the opposite case occurs: Positive LOS velocities imply subrotating flows and negative LOS velocities imply superrotating flows.

A superrotating flow is seen in Figure 3d just equatorward of the IR intensity peak of the main auroral emission at 180°–270° longitude, with positive values of LOS velocity of ~1 km/s. In a dark region of the polar aurora just poleward of the main auroral emission, there is a strongly subrotating flow with maximum LOS velocity of ~2.5 km/s. On the main auroral emission at ~90°–180° longitude, there is subrotating flow of ~1.5 km/s. The origins of these ionospheric flows are discussed in greater detail in Johnson et al. (2017).

Joule heating occurs in the auroral regions and its magnitude is governed by the difference in velocity between the charged particles and neutrals. There are very limited measurements of the neutral velocity in the thermosphere. The only two measurements of neutral winds measured in the auroral region were taken by Chaufray et al. (2010, 2011). Using observations of the H Ly-α line profile taken with HST-STIS of the northern auroral region, Chaufray et al. (2010) calculated a velocity of ~4–8 km/s at ~1,500 km above the 1-bar level. Through IR observations using the Fourier transform spectrometer (FTS/BEAR) instrument at the Canada-France Hawaii Telescope (CFHT), Chaufray et al. (2011) derived an upper limit on the LOS velocity of $<$1.0 km/s for the H_2, at altitude ~560–690 km above the 1-bar level (Uno et al., 2014). Models such as Achilleos et al. (1998), Bougher et al. (2005), and Tao et al. (2014) show that the neutral wind velocity remains less than ~1 km/s. In this paper we study H_3^+ fundamental emission that occurs at an altitude of ~550 km above the 1-bar level (Melin et al., 2005), where Chaufray et al. (2011) defined the upper limit of the neutrals to be ~1 km/s. Therefore, due to lack of further observational evidence, and small modeled velocities, we assume that the neutrals are corotating.

In such a scenario, where the neutrals are corotating, the greatest Joule heating will occur where the largest values of LOS velocities exist. Therefore, Figure 3d effectively gives a map of where the Joule heating should be occurring. Stallard et al. (2001) measured an increase in the LOS velocity in the region of the main auroral emission, from 0.5 to 1 km/s, and Stallard et al. (2002) measured an increase in temperature from 940 to 1065 K, using the same IRTF-CSHELL data set. This positive correlation between the H_3^+ ion velocity and temperature suggests increased Joule heating with increased velocity, assuming the neutrals are corotating.

The strongest ionospheric flows measured by Johnson et al. (2017) are in a dark region of the polar aurora, with an absolute magnitude of LOS velocity of up to ~2.5 km/s. Assuming the neutrals are corotating, significant Joule heating should be taking place in this region. However, Figure 3a shows that the temperatures here are moderate compared to that of the main auroral emission. Figure 7d shows the correlation between the temperature and the absolute magnitude of the LOS velocity in the PRF. There is a high occurrence of LOS velocities at 1 km/s for the temperature range of 800–950 K. The Pearson's correlation coefficient is ~0.47, implying there is a weak positive correlation, which means that there is some increase in Joule heating with velocity, as suggested by Stallard et al. (2001, 2002).

Figure 5 shows how the temperature changes over the set of observations. Section 3 explains how temperature averages 1 and 2 were created, which are ~80 min and ~50° apart. Average 1 is shown in Figure 5a, and average 2 is shown in Figure 5c. These averages were then subtracted from the average over the whole set of observations (Figure 3d), leading to the temperature differences at the start and end of the observations shown in Figures 5b and 5d, respectively. The observed temperature differences are larger than the calculated errors (Figure 6), and so these temperature changes are interpreted as physical.

Figures 5b and 5d show two broad regions of temperature changes that we will focus on. Part of the main auroral emission at ~230° longitude changes from ~50–70 K hotter than average to ~50–70 K cooler over the ~80-min separation of the two averages, labeled as region A in Figure 5. A region in the polar aurora at ~180° longitude changes from ~60 K cooler than average to ~60 K hotter over the observations, labeled region B in Figure 5. Although other small-scale variations may exist, the extended spatial coverage of regions A and B implies that they are not simply random fluctuations. In section 5.2 we will investigate two distinct hypotheses: Are the temperature changes caused by the rotation of the aurora through different local times, or are they a result of temporal changes of the conditions at Jupiter during the ~80-min separation of the two averages?

5. Discussion

5.1. H_3^+ Rotational Temperature, Column Density, and Total Emission

The energy balance in Jupiter's ionosphere is complex, and the H_3^+ parameters do not always exhibit simple correlations. Figure 7a shows that there is a strong positive correlation between the total emission (Figure 3c) and the column density (Figure 3b). Other studies, such as Stallard et al. (2002), Moore et al. (2017), and Adriani et al. (2017), also noted this correlation, and it implies that the ionization rate governs the intensity. While enhancements in H_3^+ total emission could also be caused by increases in temperature of the ionosphere, only a modest correlation between the total emission (Figure 3c) and the temperature (Figure 3a) was observed in Figure 7b. Therefore, it appears that temperature as a driver of H_3^+ emission brightness is secondary to the column density.

Although the correlation between the total emission and column density is clear, past studies have found the correlation between the total emission and temperature harder to quantify. In a study of the northern auroral region using IRTF-CSHELL observations, Stallard et al. (2002) found that the vibrational temperature had no correlation with the Q(1,0$^-$) intensity. Even though they observed high temperatures in the bright region of the main auroral emission at 180°–270° longitude, they found that at 90°–180° longitude, in the more diffuse region of the main auroral emission, the intensity was at a maximum but the temperature was at a minimum. Lam et al. (1997) and Raynaud et al. (2004) noted an anticorrelation between temperature and column density, but due to the low signal-to-noise in these studies, it was uncertain if the anticorrelation was physical. By comparing synthetic H_3^+ spectra to observations of Saturn analyzed by O'Donoghue et al. (2014), Melin et al. (2014) showed that as long as the uncertainties were small relative to the differences of temperature and column density, then the anticorrelation was physical and not caused by low signal-to-noise. Miller et al. (2010) argued that the H_3^+ thermostat effect could produce the observed anticorrelation, whereby a denser parcel of H_3^+ is subject to more cooling and will end up at a lower temperature.

Overall, Figure 7b does not show an anticorrelation, which would have implied that temperature was low where cooling by H_3^+ was high. No overall anticorrelation is seen in Figure 7c either, which shows the relationship between the temperature and column density. The recent study of Adriani et al. (2017), which uses Juno-JIRAM data, also shows no evidence of anticorrelation between the temperature and column density, in agreement with the present study. Therefore, H_3^+ is not an efficient thermostat across the entire auroral region.

One mechanism which can drive the heating of Jupiter's auroral regions is impact from particle precipitation. If heating by impact from particle precipitation was driving the elevated temperatures observed in the auroral region, then where the column density is large, the temperature would be high. However, Figure 7c shows only a modest positive relationship between temperature (Figure 3a) and column density (Figure 3b), and therefore, it seems that heating by impact from particle precipitation alone cannot be driving the heating in Jupiter's ionosphere and there must be more processes at work.

Another mechanism that drives auroral heating is Joule heating, caused by the divergence of the ionospheric and neutral flows in Jupiter's atmosphere, which are ultimately caused by the magnetosphere-ionosphere coupling currents. The model by Smith and Aylward (2009) suggested that Joule heating is largest at altitudes where conductivity is highest, which is approximately at the peak emission altitude of the H_3^+ fundamental emission lines (Millward et al., 2002). Since the height integrated current densities depend on the density of Jupiter's upper atmosphere, as the H_3^+ production increases, so does the conductivity. Millward et al. (2002) found that if the precipitating particles have energy of ~60 keV, then they will deposit their energy at an altitude where H_3^+ density is maximized (~550 km). This altitude is coincident with a region of the ionosphere where the values of ion-neutral collision frequency and the ion gyrofrequency are equal and hence the Pedersen conductivity is maximized. Stallard et al. (2001, 2002) measured a positive correlation between H_3^+ LOS velocity and temperature; however, only a weak correlation between temperature and LOS velocity was identified in this study and is shown in Figure 7d. Therefore, the temperature structure of the aurora is not directly controlled by the Joule heating.

The above discussion is for a corotating neutral thermosphere, and the temperature structure will be much more complex if neutral flows deviate from corotation. The neutrals may experience a general subrotation or superrotation, or a more complex regime of flows that differ to the ionospheric flows may exist; however, the dynamics of the neutrals at the time of the observations is not known. A more rigorous study that takes the relative LOS velocity of the neutrals and ions into account is left for future work.

Millward et al. (2002) found precipitating electron with energy ~60 keV are the most efficient at ionizing the upper atmosphere and producing H_3^+, which is very effective at producing conductivity. However, studies such as Gérard et al. (2016) and Sinclair et al. (2017) have shown that in the region of the main auroral emission precipitating electron energies are often $>$100 keV. These high energy electrons would penetrate through the upper atmosphere to ~300 km above the 1-bar level, below the homopause, where the hydrocarbons dominate and H_3^+ is readily destroyed. It could be the case that the strongest Joule heating is occurring below the peak altitude of the H_3^+ fundamental emission, and therefore, no strong correlation between temperature and LOS velocity could be detected from the H_3^+ emission.

The strong ionospheric flows observed in the northern auroral region (e.g., Johnson et al., 2017; Rego et al., 1999; Stallard et al., 2001) may also be responsible for redistributing heat. Ion drag could be responsible for redistributing neutral heat through the ion-neutral collisions, which force the neutrals to move with the ions. Achilleos et al. (2001) showed that the neutrals are strongly coupled to the ions and a circumpolar neutral jet develops with a velocity of up to ~60% of the ion velocity in the region of the main auroral emission. Past studies such as Lam et al. (1997) and Rego et al. (2000) have shown a smooth temperature gradient moving from the hot auroral region to the cooler equatorial regions. However, Stallard et al. (2017) showed that the heat transport from the northern auroral region is not uniform, and a region of localized cooling exists at the subauroral latitudes. The lifetime of H_3^+ is too short to transport heat as far as the equatorial regions. For a lifetime on the order of tens of minutes (or shorter) in the auroral regions (Achilleos et al., 1998), and a velocity of a few kilometers per second, the H_3^+ ions will move thousands to tens of thousands of kilometers across the planet. This transport could be important in redistribution of auroral energy in the polar regions. It could be the case that the strong H_3^+ ionospheric flows create regions of increased or decreased temperatures, which are not coincident with the mechanisms that drive the temperatures.

Figure 3d shows the ionospheric flows investigated by Johnson et al. (2017). In this study we will focus on the superrotating flow as it has potential consequences for the temperature structure of the auroral ionosphere. Johnson et al. (2017) discuss how the origin of the superrotating ionospheric flow could be either magnetospheric or ionospheric forcing. They suggest that this region of the ionosphere maps to a region of the magnetosphere where the flux tubes are moving radially inward as they rotate through the dawn sector of the magnetosphere. As the field lines are compressed, their rotation rate increases to conserve angular momentum, and the rotation rate of the ionosphere to which they map also increases (Moriguchi et al., 2008). Alternatively, thermospheric neutral winds could be driving the superrotational flows through collisional forcing. The model by Smith and Aylward (2009) predicts a superrotating thermospheric flow, just equatorward of the main auroral emission, caused by the zonal Coriolis and advection momentum term dominating the ion-drag term. As the model by Smith and Aylward (2009) is axisymmetric, direct comparison between their results and the observed ionospheric flows is not possible; however, it is still possible that a thermospheric superrotational flow exists near to the location of the main auroral emission, which is driving superrotational ionospheric flows.

Smith and Aylward (2009) describe how the superrotating neutral wind produces a cool region just equatorward of the main auroral emission. This cool region is caused by the divergence of a poleward flow at the boundary between the subrotating main auroral emission and the corotating lower latitude. The divergence causes an upwelling of gas from lower altitudes that cools adiabatically as it expands, creating a cool, superrotating region just equatorward of the main auroral emission. As we are assuming quasi-LTE we would expect the H_3^+ temperature to be representative of the thermosphere, and hence, we would expect to measure low temperatures. However, the opposite is observed in our data set; the region of the superrotating ionospheric flow experiences elevated H_3^+ temperatures. It could still be the case that the neutrals and H_3^+ are cooled but at lower altitudes than the peak H_3^+ emission of the fundamental lines (~550 km, Melin et al., 2005), and that this process is not captured by these observations. Alternatively, it may be that the cool region is not observed in this present study because the main auroral emission is not completely subrotating as Smith and Aylward (2009) employ in their model. Johnson et al. (2017) observed subrotational, corotational, and superrotational flows in the region of the main auroral emission, which may explain why the temperature structure is more complex in this region than predicted by Smith and Aylward (2009).

It is clear that particle precipitation impact, Joule heating, and the H_3^+ thermostat effect are not working in isolation and it is very likely that the observed temperatures are generated by a combination of the above process. More detailed studies, which measure the LOS velocities of the H_3^+ ions as well as the temperature, will further our understanding of heat transport in Jupiter's ionosphere. Furthermore, models that take the asymmetries that are observed in the temperature structure in this study into account may be able to estimate where each particular heating and cooling mechanism dominates.

5.2. H_3^+ Temperature Changes Over a Short Time Period

As discussed in section 4, two broad regions of temperature changes are observed over a period of ~80 min. We postulate that these changes could either be caused by the local time dependency of the energy of the precipitating electrons or by the response of the magnetosphere-ionosphere-thermosphere system to a transient enhancement in solar wind dynamic pressure.

First, we will consider the possibility that the temperature changes are caused by local time dependence in particle precipitation energy. The altitude of peak production of H_3^+ depends on the energy of the precipitating electrons: When the electron energy is higher, the H_3^+ will be produced at lower altitudes, and vice versa. Models such as Grodent et al. (2001) as well as observations such as Seiff et al. (1997), Uno et al. (2014), and Lystrup et al. (2008) have shown that the thermospheric temperature increases with height. Therefore, H_3^+ produced at lower altitudes will be cooler, and vice versa. It could be the case that the electron precipitation is softer in the dawn sector of the ionosphere, becoming harder at noon. Region A in Figure 5 begins hotter than average at dawn, where the electrons may be softer creating H_3^+ at higher, hotter altitudes. As it rotates towards noon, it may now be in a region in which the electron precipitation is harder, penetrating down to lower altitudes, creating H_3^+ where it is cooler. Region B starts off cool around noon, where it may be experiencing hard electron precipitation. This region becomes hotter as it moves away from noon, suggesting that the dusk sector may be subject to softer electron precipitation.

It could be the case that the aurora as a whole experienced local time differences. As discussed in section 4, the H_3^+ temperature structure measured in this present study are in agreement with those measured by Moore et al. (2017) but not Adriani et al. (2017). Moore et al. (2017) measured the dayside auroral temperatures at local times similar to those presented in this study. However, Adriani et al. (2017) derived the H_3^+ temperature from data taken over a whole Jupiter day, and the polar projections in their study are made up of measurements covering all local times. If local time differences in temperature do exist, then this would explain why the temperature structures observed in the present study agree with Moore et al. (2017) but differ from Adriani et al. (2017). In our study, we observe cooling in region A and heating in region B, which may imply that the main auroral emission and polar aurora experience different local time behavior. More generally, different morphological regions of the aurora may experience different local time behavior. However, the local time coverage of the data set is quite limited and we do not observe regions A and B at the same range of local times. Therefore, it may be that the local time differences produce the same effect in all regions of the aurora or that they change depending on the particular auroral emission component.

Tao et al. (2011) show how, due to the timescale in the ion chemistry, the H_3^+ emission rate is proportional to the square root of the precipitating electron flux. However, due to the instantaneous nature of the UV and X-ray emission, observations at these wavelengths are frequently used to probe the energy of precipitating electrons. Branduardi-Raymont et al. (2008) discuss how hard X-rays are produced from main auroral emission and soft X-rays are produced from the polar aurora. This suggests that the precipitating electrons at the main auroral emission are harder and penetrate down to lower altitudes, which would create H_3^+ where the atmosphere is cooler and vice versa for the polar aurora. The H_2 emission at wavelengths of <140 nm is attenuated by hydrocarbon absorption, which occurs at lower altitudes. By taking the ratio of the intensity of this emission to that at longer wavelengths, which is unaffected by hydrocarbon absorption, the color ratio

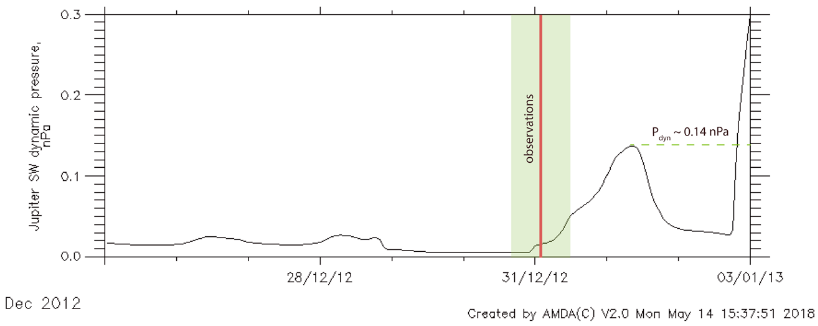

Figure 8. The propagated solar wind dynamic pressure calculated from the Tao et al. (2005) model. The plot was generated using the AMDA online tool. The observation is shown by the vertical red line and the peak in dynamic pressure closest to the observations is shown by the horizontal dashed green line. The green shaded region shows the ±20-hr error on the arrival time of the pressure enhancement at Jupiter.

can be calculated. Gérard et al. (2016) found a positive relationship between intensity and color ratio in the main auroral emission. This means that the brightest aurora is produced at lower, cooler altitudes. The relationship was less clear in the polar aurora. Although this study divided the auroral emissions by morphology, they did not investigate any local time dependence of energy of the precipitating electrons. Future simultaneous observations at IR, UV, and X-ray wavelengths could resolve the local time dependence of the energy of precipitating electrons.

Now we will consider the hypothesis that the observed H_3^+ temperature changes may be driven by temperature changes at a fixed altitude in the thermosphere. Yates et al. (2014) models the velocity and temperature of the neutral thermosphere and investigates how it responds to a transient response of the magnetosphere. They follow the description of a transient event as given by Cowley et al. (2007) who modeled the response of the magnetosphere to a rapid (2–3 hr) compression and expansion. Yates et al. (2014) trigger the transient event with a pulse of increased solar wind dynamic pressure over 3 hr, reaching 0.213 nPa halfway through the pulse. Their model shows that during and after the compression the neutral flows and temperatures in the thermosphere become highly dynamic.

At the peak emission altitude of the H_3^+ fundamental lines (~550 km, Melin et al., 2005), the modeled temperature fluctuates by ~50 K, changing from hot to cold and vice versa. In our study, the temperature changes by ~140 K, which is much higher than the temperature changes predicted by the model. Like other models, Yates et al. (2014) generally underestimates the temperatures in the auroral regions, and so it is possible that the fluctuations in temperatures are also underestimated. The model by Yates et al. (2014) is axisymmetric and therefore cannot give an exact location of the relatively large temperature changes that could be compared to the observed significant temperature changes. However, this model does show that temperature changes of the neutrals in the thermosphere are possible under the right conditions and this could also be driving the observed H_3^+ temperature changes.

To test whether this is a likely scenario for our observations, the solar wind dynamic pressure at Jupiter during these observations was investigated using a propagated solar wind model by Tao et al. (2005). The input of this model is the NASA/Goddard Space Flight Center's OMNI data set (King & Papitashvili, 2005) and the output for the timeframe surrounding the observations is shown in Figure 8. Figure 8 was generated using the AMDA (Automated Multi-Dataset Analysis) online tool (which is available at http://amda.irap.omp.eu/ [accessed 14 May 2018]). The observation time is shown by the vertical red line, and a peak in the dynamic pressure of ~0.14 nPa is shown by the horizontal dashed green line. There is a ±20-hr error on the modeled arrival time of pressure enhancements, which is represented by the green shaded region that is centered on the beginning of the enhancement in dynamic pressure. Tao et al. (2005) state that the arrival time of pressure enhancements is reasonably well predicted if the Earth-Sun-Jupiter angle is less than 50°. At the time of the observations the Earth-Sun-Jupiter angle was ~0°–5°; therefore, the arrival time of any pressure enhancements shown in Figure 8 are favorably modeled. From Nichols et al. (2017) the delay between the arrival of the pressure enhancement at the magnetopause and the impact on the ionosphere is ~3 hr. Considering the error in arrival time and the lag between arrival at magnetopause and impact on the ionosphere, the initial increase in dynamic pressure could have occurred during our observations. This increase is smaller than that which produced the dynamic response of the thermosphere as modeled by Yates et al. (2014); however, the transient response of the magnetosphere to the dynamic pressure enhancement may still be driving significant changes. It is plausible that the response of the magnetosphere and atmosphere to an increase in solar wind dynamic pressure, which triggers the changes in the neutral temperatures, drives the observed changes in the H_3^+ temperature.

To determine whether the temperature changes are driven by local time dependence in electron precipitation energy or thermospheric dynamics, further observations are required. If local time changes in electron precipitation energy are driving the temperature changes then these patterns should occur every time the aurora rotates into view and will be easily confirmed in future studies. Additionally, further observations on the nightside would allow any local time differences to be investigated there, which may be achieved with Juno measurements. The results from the transient response of the magnetosphere to solar wind dynamic pressure enhancements are likely to vary from one epoch to another. The possibility remains that both mechanisms could be driving the temperature changes and the interplay between the two processes could be causing dynamic temperature structures.

A further mechanism that may be responsible for driving the observed temperature changes could be enhanced destruction of H_3^+ at low altitudes, close to the homopause. Processes such as upwelling of stratospheric hydrocarbons cause destruction of H_3^+ at lower altitudes where the cooler population of H_3^+ exists. This would result in increased temperature being observed as only the hot population at high altitudes would remain to be detected. Upwelling of hydrocarbons may be caused by heating of the stratosphere. Sinclair et al. (2017, 2018) observed enhanced auroral stratospheric temperatures, which may cause parcels of hydrocarbons to rise and expand into the thermosphere. Future studies, which include simultaneous measurements of hydrocarbons and H_3^+ ions, may be able to determine whether enhanced destruction of H_3^+ at low altitudes drives any observed temperature changes. Finally, unknown mechanisms yet to be determined may be controlling the temperature changes.

Although this study assumes quasi-LTE, it is important to note the possibility that this is not a reasonable assumption. The fundamental emission lines are least affected by departures from LTE, and these lines are used in this paper. However, if the quasi-LTE assumption breaks down, this would likely complicate the interpretation of the H_3^+ temperature observations. In order to fully test temperature changes, one would need to measure the kinetic and vibrational temperatures of the H_3^+, in addition to the rotational temperature as measured in this study, to ascertain whether H_3^+ was in LTE. However, these measurements are outside the scope of this study.

6. Conclusions

This study has presented high spatial resolution polar projections of the total emission, column density, and temperature of H_3^+ in Jupiter's northern auroral region observed on 31 December 2012 using VLT-CRIRES. A comparison of these parameters, as well as the previously measured LOS velocity (Johnson et al., 2017), was undertaken and has shown that the heating mechanisms that control the temperature of Jupiter's thermosphere are not simple.

The strong positive correlation between column density and total emission, and the lack of a clear relationship between temperature and total emission, suggests that spatial variations of the H_3^+ auroral emission are dominated by ionization (i.e., production) rather than H_3^+ brightness enhancements being caused by increased temperatures. Since no significant correlation between temperature and total emission was found, it appears that H_3^+ is not an efficient thermostat across the whole auroral region. This study found no clear relationship between the column density and temperature, suggesting that impact from particle precipitation does not dominate heating in the auroral regions. Although elevated temperatures were found in some regions with strong ionospheric flows, only a weak correlation was found between the LOS velocity and the temperature.

The heating of Jupiter's upper atmosphere appears to be controlled by a combination of energy being reradiating to space by H_3^+ and heating by impact from particle precipitation and Joule heating. Since the lifetime of the H_3^+ ions is not negligible, strong H_3^+ ionospheric flows may be able to transport heat around the auroral region, meaning that the original driving mechanism may exist in a different region from the observed elevated temperatures.

This study is the first to present H_3^+ temperature changes over a short period of time, and we proposed two mechanisms to explain the observed temperature changes. First, the temperature changes could be caused by local time changes in particle precipitation energy, which could vary by morphology region in the aurora or affect the auroral regions as a whole. However, due to the limited local time range of the observations we cannot distinguish between either case. Second, the temperature changes could be due to the dynamics of the thermospheric neutrals. A model by Yates et al. (2014) has shown that the temperatures and winds of the thermospheric neutrals respond dynamically to the transient response of the magnetosphere caused by a solar wind dynamic pressure enhancement. From propagated solar wind parameters (Tao et al., 2005), it was found that a pressure enhancement could have arrived during the observations inside the ±20-hr error window on arrival time. This could have caused dynamic temperature structures in the thermosphere, which drive the observed temperature changes in the ionosphere.

We have presented a case study of Jupiter's northern ionosphere, and to answer the remaining open questions, further studies are required. If the temperature changes observed here are repeatedly identified at similar local times in future studies, then local time changes in particle precipitation energy will be very likely causing the changes in temperature. Changes in temperature due to transient dynamic thermospheric behavior will vary depending on the solar wind conditions, and it will be important to observe Jupiter's aurora with spacecraft in situ upstream of Jupiter in the solar wind. In future studies, it will also be important to test the validity of the LTE assumption by simultaneously measuring the rotational, vibrational, and kinetic temperatures of H_3^+. This will help determine the extent to which H_3^+ is thermalized with the neutrals. Additionally, by simultaneously observing the temperature and LOS velocity of the neutrals, their effect on the temperature structure of the ionosphere could potentially be determined.

Acknowledgments

This study is based on observations collected at the European Organization for Astronomical Research in the Southern Hemisphere under ESO programme 090.C-0353(A). VLT spectral data are available from the ESO Science Archive Facility. The propagated solar wind model by Tao et al. (2005) with the OMNI data set input is available through the AMDA science analysis system provided by the Centre de Données de la Physique des Plasmas (CDPP) supported by CNRS, CNES, Observatoire de Paris, and Université Paul Sabatier, Toulouse. R. E. J. and M. N. C. were supported by the UK Science and Technology Facilities Council (STFC) studentships. H. M., T. S. S., and J. D. N. were supported by the STFC grant ST/N000749/1. C. T. acknowledges support from JSPS KAKENHI grant 15K17769.

References

Achilleos, N., Miller, S., Prangé, R., Millward, G., & Dougherty, M. K. (2001). A dynamical model of Jupiter's auroral electrojet. *New Journal of Physics*, *3*(3), 1–21. https://doi.org/10.1088/1367-2630/3/1/001

Achilleos, N., Miller, S., Tennyson, J., Aylward, A. D., Mueller-Wodarg, I., & Rees, D. (1998). JIM: A time-dependent, three-dimensional model of Jupiter's thermosphere and ionosphere. *Journal of Geophysical Research*, *103*(E9), 20,089–20,112. https://doi.org/10.1029/98JE00947

Adriani, A., Mura, A., Moriconi, M. L., Dinelli, B. M., Fabiano, F., Altieri, F., et al. (2017). Preliminary JIRAM results from Juno polar observations: 2. Analysis of the Jupiter southern H_3^+ emissions and comparison with the north aurora. *Geophysical Research Letters*, *44*, 4633–4640. https://doi.org/10.1002/2017GL072905

Bougher, S. W., Hunter Waite, J., Majeed, T., & Randy Gladstone, G. (2005). Jupiter Thermospheric general circulation model (JTGCM): Global structure and dynamics driven by Auroral and joule heating. *Journal of Geophysical Research*, *110*, A04008. https://doi.org/10.1029/2003JE002230

Branduardi-Raymont, G., Elsner, R. F., Galand, M., Grodent, D., Cravens, T. E., Ford, P., et al. (2008). Spectral morphology of the X-ray emission from Jupiter's aurorae. *Journal of Geophysical Research*, *113*, A02202. https://doi.org/10.1029/2007JA012600

Chaufray, J. Y., Gladstone, G. R., Waite, J. H., & Clarke, J. T. (2010). Asymmetry in the Jovian auroral Lyman-α line profile due to thermospheric high-speed flow. *Journal of Geophysical Research*, *115*, E05002. https://doi.org/10.1029/2009JE003439

Chaufray, J.-Y., Greathouse, T. K., Gladstone, G. R., Waite, J. H. Jr., Maillard, J.-P., Majeed, T., et al. (2011). Spectro-imaging observations of Jupiter's 2μm auroral emission. II: Thermospheric winds. *Icarus*, *211*, 1233–1241. https://doi.org/10.1016/j.icarus.2010.11.021

Cowley, S. W. H., Alexeev, I. I., Belenkaya, E. S., Bunce, E. J., Cottis, C. E., Kalegaev, V. V., et al. (2005). A simple axisymmetric model of magnetosphere-ionosphere coupling currents in Jupiter's polar ionosphere. *Journal of Geophysical Research*, *110*, A11209. https://doi.org/10.1029/2005JA011237

Cowley, S. W. H., & Bunce, E. J. (2001). Origin of the main auroral oval in Jupiter's coupled magnetosphere–ionosphere system. *Planetary and Space Science*, *49*(10-11), 1067–1088. https://doi.org/10.1016/S0032-0633(00)00167-7

Cowley, S. W. H., Nichols, J. D., & Andrews, D. J. (2007). Modulation of Jupiter's plasma flow, polar currents, and auroral precipitation by solar wind-induced compressions and expansions of the magnetosphere: A simple theoretical model. *Annales Geophysicae*, *25*(6), 1433–1463. https://doi.org/10.5194/angeo-25-1433-2007

Drossart, P., Maillard, J.-P., Caldwell, J., Kim, S. J., Watson, J. K. G., Majewski, W. A., et al. (1989). Detection of H_3^+ on Jupiter. *Nature*, *340*(6234), 539–541. https://doi.org/10.1038/340539a0

Gérard, J.-C., Bonfond, B., Grodent, D., & Radioti, A. (2016). The color ratio-intensity relation in the Jovian aurora: Hubble observations of auroral components. *Planetary and Space Science*, *131*, 14–23. https://doi.org/10.1016/j.pss.2016.06.004

Giles, R. S., Fletcher, L. N., Irwin, P. G. J., Melin, H., & Stallard, T. S. (2016). Detection of H_3^+ auroral emission in Jupiter's 5-micron window. *Astronomy & Astrophysics*, *589*, 3–7. https://doi.org/10.1051/0004-6361/201628170

Grodent, D., Bonfond, B., Gérard, J. C., Radioti, A., Gustin, J., Clarke, J. T., et al. (2008). Auroral Evidence of a Localized Magnetic Anomaly in Jupiter's Northern Hemisphere. *Journal of Geophysical Research*, *113*, A09201. https://doi.org/10.1029/2008JA013185

Grodent, D., Waite, J. H., & Gerard, J. C. (2001). A self-consistent model of the Jovian auroral structure. *Journal of Geophysical Research*, *106*(A7), 12,933–12,952. https://doi.org/10.1029/2000JA900129

Hill, T. W. (2001). The Jovian auroral oval. *Journal of Geophysical Research*, *106*(A5), 8101–8107. https://doi.org/10.1029/2000JA000302

Johnson, R. E., Stallard, T. S., Melin, H., Nichols, J. D., & Cowley, S. W. H. (2017). Jupiter's polar ionospheric flows: High resolution mapping of spectral intensity and line-of-sight velocity of H_3^+ ions. *Journal of Geophysical Research: Space Physics*, *122*, 7599–7618. https://doi.org/10.1002/2017JA024176

Kaufl, H. U., Ballester, P., Biereichel, P., Delabre, B., Donaldson, R., Dorn, R., et al. (2004). CRIRES: A high resolution infrared spectrograph for ESO's VLT. *SPIE*, *5492*, 1218–1227. https://doi.org/10.1117/12.551480

Kim, Y. H., Fox, J. L., & Porter, H. S. (1992). Densities and vibrational distribution of H_3^+ in the Jovian auroral ionosphere. *Journal of Geophysical Research*, *97*(E4), 6093–6101. https://doi.org/10.1029/92JE00454

King, J. H., & Papitashvili, N. E. (2005). Solar wind spatial scales in and comparisons of hourly wind and ACE plasma and magnetic field data. *Journal of Geophysical Research*, *110*, A02104. https://doi.org/10.1029/2004JA010649

Lam, H. A., Achilleos, N., Miller, S., Tennyson, J., Trafton, L. M., Geballe, T. R., & Ballester, G. E. (1997). A baseline spectroscopic study of the infrared auroras of Jupiter. *Icarus*, *127*, 379–393.

Lystrup, M. B., Miller, S., Dello Russo, N., Vervack, R. J. Jr., & Stallard, T. (2008). First vertical ion density profile in Jupiter's auroral atmosphere: Direct observations using the Keck II telescope. *The Astrophysical Journal*, *677*(1), 790–797. https://doi.org/10.1086/529509

McCall, Benjamin John (2001). Spectroscopy of H_3^+ in laboratory and astrophysical plasmas, (PhD thesis). University of Chicago, Chicago, IL.

Melin, H., Stallard, T. S., O'Donoghue, J., Badman, S. V., Miller, S., & Blake, J. S. D. (2014). On the anticorrelation between H_3^+ temperature and density in giant planet ionospheres. *Monthly Notices of the Royal Astronomical Society*, *438*(2), 1611–1617. https://doi.org/10.1093/mnras/stt2299

Melin, H., Miller, S., Stallard, T., & Grodent, D. (2005). Non-LTE effects on H_3^+ emission in the Jovian upper atmosphere. *Icarus*, *178*(1), 97–103. https://doi.org/10.1016/j.icarus.2005.04.016

Melin, H., Miller, S., Stallard, T., Smith, C., & Grodent, D. (2006). Estimated energy balance in the Jovian upper atmosphere during an auroral heating event. *Icarus*, *181*(1), 256–265. https://doi.org/10.1016/j.icarus.2005.11.004

Melin, H., & Stallard, T. S. (2016). Jupiter's hydrogen bulge: A Cassini perspective. *Icarus*, *278*, 238–247. https://doi.org/10.1016/j.icarus.2016.06.023

Miller, S., Achilleos, N., Ballester, G. E., Lam, H. A., Tennyson, J., Geballe, T. R., & Trafton, L. M. (1997). Mid-to-low latitude H_3^+ emission from Jupiter. *Icarus*, *130*(1), 57–67. https://doi.org/10.1006/icar.1997.5813

Miller, S., Joseph, R. D., & Tennyson, J. (1990). Infrared emissions of H3 (+) in the atmosphere of Jupiter in the 2.1 and 4.0 micron region. *The Astrophysical Journal*, *360*, L55–L58. https://doi.org/10.1086/185811

Miller, S., Stallard, T., Melin, H., & Tennyson, J. (2010). H3+ cooling in planetary atmospheres. *Faraday Discussions*, *147*, 283–291. https://doi.org/10.1039/c004152c

Miller, S., Stallard, T., Smith, C., Millward, G., Melin, H., Lystrup, M., & Aylward, A. (2006). H3+: The driver of giant planet atmospheres. *Philosophical Transactions. Series A, Mathematical, Physical, and Engineering Sciences*, *364*(1848), 3121–3137. https://doi.org/10.1098/rsta.2006.1877

Miller, S., Stallard, T., Tennyson, J., & Melin, H. (2013). Cooling by H3+ emission. *The Journal of Physical Chemistry A*, *117*(39), 9770–9777. https://doi.org/10.1021/jp312468b

Millward, G., Miller, S., Stallard, T., Aylward, A.~D., & Achilleos, N. (2002). On the dynamics of the Jovian ionosphere and thermosphere III. The modelling of Auroral conductivity. *Icarus*, *160*(1), 95–107. https://doi.org/10.1006/icar.2002.6951

Moore, L., Melin, H., Stallard, T., Tao, C., Zieger, B., Clarke, J., et al. (2017). Variability of Jupiter's IR H3+ aurorae during Juno approach. *Geophysical Research Letters*, *44*(10), 4513–4522. https://doi.org/10.1002/2017GL073156

Moriguchi, T., Nakamizo, A., Tanaka, T., Obara, T., & Shimazu, H. (2008). Current systems in the Jovian magnetosphere. *Journal of Geophysical Research*, *113*, A05204. https://doi.org/10.1029/2007JA012751

Neale, L., Miller, S., & Tennyson, J. (1996). Spectroscopic properties of the H3+ molecule: A new calculated line list. *The Astrophysical Journal*, *464*, 516–520. https://doi.org/10.1086/177341

Nichols, J. D., Badman, S. V., Bagenal, F., Bolton, S. J., Bonfond, B., Bunce, E. J., et al. (2017). Response of Jupiter's auroras to conditions in the interplanetary medium as measured by the Hubble space telescope and Juno. *Geophysical Research Letters*, *44*, 7643–7652. https://doi.org/10.1002/2017GL073029

O'Donoghue, J., Stallard, T. S., Melin, H., Cowley, S. W. H., Badman, S. V., Moore, L., et al. (2014). Conjugate observations of Saturn's northern and southern H3+ aurorae. *Icarus*, *229*, 214–220. https://doi.org/10.1016/j.icarus.2013.11.009

Raynaud, E., Lellouch, E., Maillard, J. P., Gladstone, G. R., Waite, J. H., B??zard, B., et al. (2004). Spectro-imaging observations of Jupiter's 2 micron auroral emission. I. H3+ distribution and temperature. *Icarus*, *171*(1), 133–152. https://doi.org/10.1016/j.icarus.2004.04.020

Rego, D., Miller, S., & Achilleos, N. (2000). Latitudinal profiles of the Jovian IR emissions of H3+ at 4 Mm with the NASA infrared telescope facility: Energy inputs and thermal balance. *Icarus*, *147*(2), 366–385. https://doi.org/10.1006/icar.2000.6444

Rego, D., Achilleos, N., Stallard, T., Steve Miller, R. P., Dougherty, M., & Joseph, R. D. (1999). Supersonic winds in Jupiter's aurorae. *Nature*, *399*(6732), 121–124. https://doi.org/10.1038/20121

Seiff, A., Kirk, D. B., Knight, T. C. D., Young, L. A., Milos, F. S., Venkatapathy, E., et al. (1997). Thermal structure of Jupiter's upper atmosphere derived from the Galileo probe. *Science*, *276*(5309), 102–104. https://doi.org/10.1126/science.276.5309.102

Sinclair, J. A., Orton, G. S., Greathouse, T. K., Fletcher, L. N., Moses, J. I., Hue, V., & Irwin, P. G. J. (2017). Jupiter's Auroral-related stratospheric heating and chemistry I: Analysis of voyager-IRIS and Cassini-CIRS spectra. *Icarus*, *292*, 182–207. https://doi.org/10.1016/j.icarus.2016.12.033

Sinclair, J. A., Orton, G. S., Greathouse, T. K., Fletcher, L. N., Moses, J. I., Hue, V., & Irwin, P. G. J. (2018). Jupiter's auroral-related stratospheric heating and chemistry II: Analysis of IRTF-TEXES spectra measured in December 2014. *Icarus*, *300*, 305–326. https://doi.org/10.1016/j.icarus.2017.09.016

Smith, C. G. A., & Aylward, A. D. (2009). Coupled rotational dynamics of Jupiter's thermosphere and magnetosphere. *Annales de Geophysique*, *27*(1), 199–230. https://doi.org/10.5194/angeo-27-199-2009

Southwood, D. J., & Kivelson, M. G. (2001). A new perspective concerning the influence of the solar wind on the Jovian magnetosphere. *Journal of Geophysical Research*, *106*(A4), 6123–6130. https://doi.org/10.1029/2000JA000236

Stallard, T., Miller, S., Millward, G., & Joseph, R. D. (2002). On the dynamics of the Jovian ionosphere and thermosphere II. The measurement of H3+ vibrational temperature, column density, and Total emission. *Icarus*, *156*(2), 498–514. https://doi.org/10.1006/icar.2001.6793

Stallard, T., Miller, S., Millward, G., & Joseph, R. D. (2001). On the dynamics of the Jovian ionosphere and thermosphere I: The measurement of ion winds. *Icarus*, *154*(2), 475–491. https://doi.org/10.1006/icar.2001.6681

Stallard, T. S., Melin, H., Miller, S., Moore, L., O'Donoghue, J., Connerney, J. E. P., et al. (2017). The great cold spot in Jupiter's upper atmosphere. *Geophysical Research Letters*, *44*, 3000–3008. https://doi.org/10.1002/2016GL071956

Tao, C., Badman, S. V., & Fujimoto, M. (2011). UV and IR auroral emission model for the outer planets: Jupiter and Saturn comparison. *Icarus*, *213*(2), 581–592. https://doi.org/10.1016/j.icarus.2011.04.001

Tao, C., Kataoka, R., Fukunishi, H., Takahashi, Y., & Yokoyama, T. (2005). Magnetic field variations in the Jovian magnetotail induced by solar wind dynamic pressure enhancements. *Journal of Geophysical Research*, *110*, A11208. https://doi.org/10.1029/2004JA010959

Tao, C., Miyoshi, Y., Achilleos, N., & Hajime, K. (2014). Response of the Jovian thermosphere to variations in solar FUV flux. *Journal of Geophysical Research: Space Physics*, *119*, 3664–3682. https://doi.org/10.1002/2013JA019411

Uno, T., Kasaba, Y., Tao, C., Sakanoi, T., Kagitani, M., Fujisawa, S., et al. (2014). Vertical emissivity profiles of Jupiter's northern H3+ and H2 infrared auroras observed by Subaru/IRCS. *Journal of Geophysical Research: Space Physics*, *119*, 10,219–10,241. https://doi.org/10.1002/2014JA020454

Yates, J. N., Achilleos, N., & Guio, P. (2014). Response of the Jovian thermosphere to a transient 'pulse' in solar wind pressure. *Planetary and Space Science*, *91*, 27–44. https://doi.org/10.1016/j.pss.2013.11.009

Yelle, R. V., & Miller, S. (2004, 218). Jupiter's thermosphere and ionosphere. In F. Bagenal, T. Dowling, & W. McKinnon (Eds.), *Jupiter: The planet, satellites and magnetosphere*, (chap. 9, 1st ed., pp. 182–218). Cambridge, UK: Cambridge University Press: Cambridge Planetary Science. http://www.cambridge.org/us/academic/subjects/astronomy/planetary-science/jupiter-planet-satellites-and-magnetosphere

Zieger, B., Tóth, G., Opher, M., & Gombosi, T. (2015). Solar wind prediction at Pluto during the new horizons flyby: Results from a two-dimensional multifluid MHD model of the outer heliosphere. Abstract SM31D-2539 Presented at 2015 Fall Meeting.